Transport in Porous Media (2005) 60:183–197
DOI 10.1007/s11242-004-5129-5
© Springer 2005

Stability of Solutal Convection in a Gravity Modulated Mushy Layer During the Solidification of Binary Alloys

S. K. PILLAY[1] and S. GOVENDER[2,*]
[1]*Sasol Limited, Synfuels, Secunda 2302, South Africa*
[2]*School of Mechanical Engineering, University of Kwa-Zulu Natal, Durban 4041, South Africa*

(Received: 5 July 2004; accepted in final form 17 November 2004)

Abstract. The linear stability theory is used to investigate analytically the effects of gravity modulation on solutal convection in the mushy layer of solidifying binary alloys. The gravitational field consists of a constant part and a sinusoidally varying part, which is synonymous to a vertically oscillating mushy layer subjected to constant gravity. The linear stability results are presented for both the synchronous and subharmonic solutions. It is demonstrated that up to the transition point between the synchronous and subharmonic regions, increasing the frequency of vibration rapidly stabilizes the solutal convection. Beyond the transition point, further increases in the frequency tend to destabilize the solutal convection, but gradually. It is also demonstrated that the effect of increasing the ratio of the Stefan number and the solid composition (η_o) is to destabilize the solutal convection.

Key words: gravity modulation, mushy layer, binary alloy, solutal convection, Rayleigh number.

Nomenclature

Latin symbols

b_* vibration amplitude.
C dimensionless composition, equals, $C_* - C_o/\Delta C$.
$\hat{e}_x$ unit vector in the x-direction.
$\hat{e}_y$ unit vector in the y-direction.
$\hat{e}_z$ unit vector in the z-direction.
D solutal diffusivity.
Da Darcy number, equals Π_{o*}/H_*.
Fr Froude number, equals $\lambda_*^2/(g_* H_*^3)$.
g_* gravitational acceleration, $9.81\,\mathrm{m/s^2}$
h_{fs} latent heat of solidification.
H_* the height of the mushy layer.

*Author for correspondence: e-mail: govenders65@nu.ac.za

Π_0 characteristic permeability of mushy layer.
k thermal conductivity.
Π_* variable permeability of the mushy layer.
l_{λ^*} thermal diffusion length, equals λ_*/V_{f*}.
L_* the length of the mushy layer.
Le Lewis number, equals λ_*/D_f
p dimensionless reduced pressure.
Pr Prandtl number, equals ν_*/λ_*.
q specific heat per unit volume.
Ra_m porous media gravitational Rayleigh number, equals, $\Pi_0\beta_{c*}g_*\Delta C/\nu_* V_{f*}$.
s convection wavenumber.
St Stefan number, equals $h_{fs}/q_s\Delta T$.
t_* time.
T dimensionless temperature, equals, $(T_* - T_L(C_o))/\Delta T$.
u horizontal x component of the filtration velocity.
v horizontal y component of the filtration velocity.
w vertical z component of the filtration velocity.
$\boldsymbol{V}$ dimensionless filtration velocity vector, equals $u\hat{\boldsymbol{e}}_x + v\hat{\boldsymbol{e}}_y + w\hat{\boldsymbol{e}}_z$.
V_{f*} Front/solidification velocity.
$\boldsymbol{X}$ space vector, equals $x\hat{e}_x + y\hat{e}_y + z\hat{e}_z$.
x horizontal length coordinate.
y horizontal width coordinate.
z vertical coordinate.

Greek symbols

α parameter related to the wave number, equals s^2/π^2.
β_T thermal expansion coefficient.
β_c solutal expansion coefficient.
γ equals χ_o/π^2.
δ dimensionless depth of mushy layer, equals H_*/l_{λ^*}.
Λ equals, $\kappa Fr\Omega^2$.
ΔC characteristic composition difference, equals $C_o - C_E$.
ΔT characteristic temperature difference, equals $T_L(C_o) - T_E$.
φ volume fraction of solid dendrites (solid fraction).
ϕ porosity, equals $(1-\varphi)$.
κ b_*/H_*.
λ_* effective thermal diffusivity.
μ_* fluid dynamic viscosity.
ρ density.
σ Growth factor.
χ_o modified Darcy–Prandtl number, equals $\mathrm{Pr}(l^2_{\kappa*}\Pi_0)$.
χ equals $\delta^2\chi_o = Da/Pr$.
υ_* fluid kinematic viscosity.
$\Pi(\phi)$ Retardability function, equals Π_0/Π_*.
η_o equals $1 + \tilde{S}/C_s$.
ω_* vibration frequency.
ϑ_o mobility ratio, equals l^2_{k*}/Π_0.
Ω scaled vibration frequency, equals, $\delta^2\omega^2_*\lambda_*/V^2_{f*}$.
Γ slope of liquidus line.
ζ composition ratio, equals $(C_s - C_o)/\Delta C$.
ξ scaled growth factor, equals $\sigma/\sqrt{-a}$.

Subscripts

*	dimensional values.
B	basic state.
c	characteristic.
C	classic.
cr	critical values.
eff	effective values.
E	related to eutectic values.
l	related to the liquid melt.
m	related to the mushy layer parameters.
M	modified.
o	related to unmodulated quantities.
s	related to the solid layer.

Superscripts

$\sim$	scaled quantities.
$\wedge$	scaled quantities.

1. Introduction

Alloyed components are widely used in demanding and critical applications, such as turbine blades, and a consistent internal structure is paramount to the performance and integrity of the component. The internal structure of an alloy traces back to its solidification from the liquid melt phase. Alloys are susceptible to the formation of vertical channels of a composition different to the surrounding solid known as freckles. Copey *et al*. (1970) initially proposed the origin of the freckles and many experiments including those in ammonium chloride by Chen and Chen (1991), and Tait and Jaupart (1992) investigated various modes of convection and the relation to freckle formation. Fowler (1985) proposed a model for the mushy layer and analysed it for the limiting case when the mushy layer behaved like a non-reacting porous layer. Amberg and Homsey (1993) conducted a weak non-linear analysis of convection in a mushy layer. Amberg and Homsey (1993) differed from Fowler (1985) in that the mushy layer was now decoupled from the liquid melt and the solid layer and perturbations were used to re-introduce the effects of permeability to develop a less limiting case. Anderson and Worster (1995, 1996) extended the model of Amberg and Homsey (1993), adopting large Stefan number scaling and observed another oscillatory mode of convection different to the double diffusive mode observed by Chen *et al*. (1994). A mushy layer, including rotational effects, for a Stefan number of $O(1)$ was investigated by Govender and Vadasz (2002). It was observed that rotation stabilizes solutal convection in the mushy layer.

Recently, Govender (2004a) analysed the stability of free convection in a vertically modulated porous layer subjected to constant vertical stratification, i.e. modulated Rayleigh–Benard convection and thereafter went on to further analyse, Govender (2004b), the actual transition point from

synchronous to subharmonic solutions. The objective of the current work is to analyse the stability of solutal convection in a mushy layer during the solidification of binary alloys subject to a similar vertical stratification.

2. Problem Formulation

A binary alloy melt, cooled from below, subject to vibration parallel to the gravitational field in the vertical direction, is presented in Figure 1. The solidification process results in three distinct regions forming viz. the solid region, of a temperature below the eutectic temperature T_E, a liquid melt region, with a temperature above the liquidus temperature $T_L(C_o)$ and a mushy layer sandwiched between the solid layer and the liquid melt.

The composition at the mush-liquid interface is C_o and the composition at the mush-solid interface is C_E. We propose that the mush-liquid interface and the mush-solid interface advances at a constant speed V_{f*} implying that the binary alloy is directionally cast and the mushy layer is of constant height H_* and width L_*, similar to the model of Amberg and Homsey (1993) and Govender and Vadasz (2002).

This results in the mushy layer having rigid and isothermal upper and lower boundary conditions where the vertical components of velocity is zero, physically isolating and dynamically decoupling the mushy layer from the solid region below and the liquid melt above. Subject to these

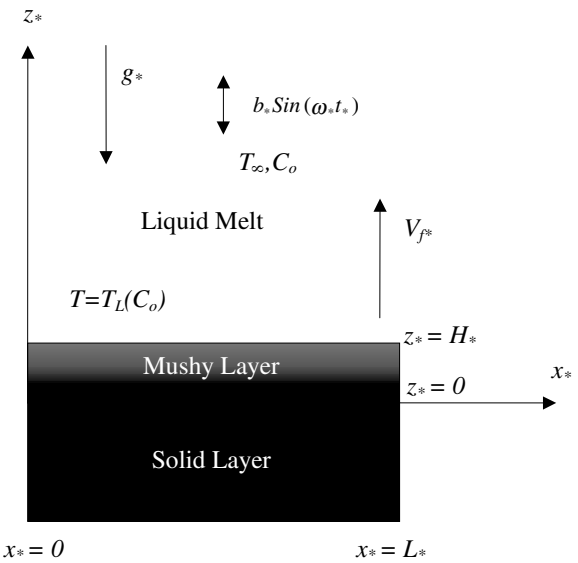

Figure 1. A schematic of the proposed problem showing the imposed boundary conditions.

conditions, and performing a transformation for the translating frame of reference (for solidification), the following dimensional set of governing equations for continuity, energy, solute and Darcy, are proposed

$$\nabla_* \cdot \boldsymbol{V}_* = 0, \tag{1}$$

$$q\left(\frac{\partial}{\partial t_*} - V_{f*}\frac{\partial}{\partial z_*}\right) T_* + q_f \boldsymbol{V}_* \cdot \nabla_* T_* = \nabla_* \cdot (k_m \nabla_* T_*) + h_{fs}\left(\frac{\partial}{\partial t_*} - V_{f*}\frac{\partial}{\partial z_*}\right)\varphi, \tag{2}$$

$$(1-\varphi)\left(\frac{\partial}{\partial t_*} - V_{f*}\frac{\partial}{\partial z_*}\right) C_* + \boldsymbol{V}_* \cdot \nabla T = \nabla_* \cdot (D_m \nabla_* \cdot T_*) + (C_* - C_S)\left(\frac{\partial}{\partial t_*} - V_{f*}\frac{\partial}{\partial z_*}\right)\varphi, \tag{3}$$

$$\frac{1}{(1-\varphi)}\left(\frac{\partial}{\partial t_*} - V_{f*}\frac{\partial}{\partial z_*}\right)\boldsymbol{V}_* + \frac{\mu_*}{\Pi_*}\frac{1}{\rho_*}\boldsymbol{V}_* = \frac{-1}{\rho_*}\nabla_* p_* + \rho_*(g_* + b_*\omega_* \mathrm{Sin}(\omega_* t_*))\hat{e}_g. \tag{4}$$

In Equations (1–4), $\boldsymbol{V}_*$ is the filtration velocity in the mush, T_* is the dimensional temperature, φ is the solid fraction, C_* is the composition, p_* is the reduced pressure, and $\hat{e}_g$ is the unit vector in the direction of gravity. In Equation (4), b_* and ω_* refers to the amplitude and frequency of the imposed vibration. The specific heat per unit volume (q) and the mush thermal conductivity (k_m) of the mushy layer are given as $q_{eff} = \varphi q_s + (1-\varphi)q_l$ and $k_{eff} = \varphi k_s + (1-\varphi)k_l$, respectively. Taking $q_s \approx q_l$ and $k_s \approx k_l$ yields $q = q_s = q_l$ and $k_m = k_s = k_l$. The linear liquidus relation is defined as $T = (T_* - T_L(C_o))/\Delta T$ and $C = (C_* - C_o)/\Delta C$ where $\Delta T = T_L(C_o) - T_E$, $\Delta C = C_o - C_E$, $\Delta T = \Gamma \Delta C$. The Boussinesq approximation is made and consists of setting $\rho_* = \rho_{o*}$ except in buoyancy terms emanating from body forces in the Darcy equation. The Boussinesq approximation and linear liquidus relation allow us to define a linear density ρ_l to composition C_* relation in a similar fashion to Govender and Vadasz (2002) with $\rho_l = \rho_{o*}(1 - \beta_{T*}(T_* - T_E) + \beta_{C*}(C_* - C_o))$. Note that $\beta_{C*} \gg \beta_{T*}$ as density is a stronger function of composition than temperature and the density equation can simplify to $\rho_l - \rho_{o*} = \rho_{o*}\beta_{C*}(C_* - C_o)$. This allows us to focus on solutal effects on convection without greatly sacrificing accuracy. The linear liquidus relation gives $C_* - C_o = T\Delta C$ further simplifying the density equation to $\rho_l - \rho_{o*} = \rho_{o*}\beta_{C*} T \Delta C$. The scaling variables $\boldsymbol{V}_*$, λ_*/V_{f*}, λ_*/V_{f*}^2, and $\lambda_* \mu^*/\Pi_0$ are used to non-dimensionlise the filtration velocity, length, time and pressure components, respectively, and the following system of

dimensionless governing equations result,

$$\nabla \cdot \boldsymbol{V} = 0, \tag{5}$$

$$\left(\frac{\partial}{\partial t} - \frac{\partial}{\partial z}\right)(T - St\varphi) + \boldsymbol{V} \cdot \nabla T = \nabla^2 T, \tag{6}$$

$$\left(\frac{\partial}{\partial t} - \frac{\partial}{\partial z}\right)((1-\varphi)T - \varsigma\varphi) + \boldsymbol{V} \cdot \nabla T = \frac{1}{Le}\nabla\left((1-\varphi)\nabla T\right), \tag{7}$$

$$\frac{1}{(1-\varphi)\chi_o}\left(\frac{\partial}{\partial t} - \frac{\partial}{\partial z}\right)\boldsymbol{V} + \Pi(\varphi)\boldsymbol{V} = -\nabla p - Ra_m\left[1 + \Lambda\sin(\Omega t)\right]T\hat{e}_z. \tag{8}$$

A number of dimensionless parameters emanate from the dimensionless analysis. In Equation (6), St is the Stefan number, and represents the ratio of the latent heat (h_{fs}) to heat content or internal energy, and is defined as $St = h_{fs}/\left(q_{eff}\Delta T\right)$. One also observe the Lewis number, Le, in Equation (7), which represents the ratio of thermal to solutal diffusivity and is defined as $Le = \lambda_*/D_f$. The effective thermal diffusivity λ_* is defined as the ratio of the thermal conductivity and the specific heat per unit volume $\lambda_* = k_{eff}/q_{eff}$. The composition ratio ς, in Equation (7), relates the differences in the characteristic compositions of the liquid and solid phases with the varying composition of the liquid within the mushy layer, and is defined as $\varsigma = (C_s - C_o)/(C_o - C_E)$. In the case of solidifying binary alloys, the Lewis number, Le, usually assumes large values thereby resulting in the right hand side of Equation (7) becoming negligible. Equation (7) may therefore be reduced to,

$$\left(\frac{\partial}{\partial t} - \frac{\partial}{\partial z}\right)((1-\varphi)T - \varsigma\varphi) + \boldsymbol{V} \cdot \nabla T = 0, \tag{9}$$

for large Lewis numbers. In Equation (8), the modified Darcy-Prandtl number (defined as $\chi_o = \mathrm{Pr}\vartheta_o$), relevant to solidification-type problems, normally assumes small values for binary alloy mixtures, see Vadasz (1998) and is thereby resulting in the retention of the time derivative in the Darcy equation. The mushy layer Rayleigh number Ra_m is defined as $Ra_m = \Pi_0\beta_{c*}g_*\Delta C/\nu_* V_{f*}$. Note that μ_* refers to the dynamic viscosity, ρ_* is the density, and g_* is the gravitational acceleration.

In Equation (8), the retardability function, as proposed by Nield (1999), is defined as $\Pi(\varphi) = \Pi_0/\Pi_*$ (where Π_0 is the characteristic permeability and Π_* is the permeability of the mushy layer), and the dimensional amplitude Λ is defined as $\Lambda = (\kappa \cdot Fr_M)\cdot\Omega^2$ (where $\kappa = b_*/H_*$ and $\Omega = (\delta^2\omega_*\lambda_*)/V_{f*}^2$). The modified Froude number, Fr_M, proposed by Govender for solidifying binary alloy systems is given as $Fr_M = \lambda_*/\left(H_*^3 g_*\right) = Fr_C\delta^2$, where Fr_C is the classic Froude Number, $Fr_C = V_{f*}/(H_* g_*)$ defined in terms of the front velocity, gravitational acceleration and the mushy layer height. For a binary alloy system such as brass (70% Copper–30% Zinc), the thermal diffusivity

is $\lambda_* = 34.2 \times 10^{-6} m^2/s$, whilst for a ammonium salt–water system (NH_4Cl–H_2O), the thermal diffusivity is of the order $\lambda_* = 0.147 \times 10^{-6} m^2/s$. If the mushy layer height is taken to be $H_* = 5\,\text{mm}$, the modified Froude numbers for the alloy system and the salt-water system may be approximated to be $Fr_{M,Brass} = 0.000954$, and $Fr_{M,Salt-Water} = 1.762 \times 10^{-8}$. Using the relationship between the classic and modified Froude numbers one may evaluate the solidification front velocities for the alloy and salt–water system (for $\delta = 0.1$) to be $V_{f*,Brass} = 0.0684\,\text{cm/s}$ and $V_{f*,Salt-Water} = 6.44 \times 10^{-4}\,\text{cm/s}$. It should be pointed out that Chen *et al.* (1994), in their lab experiments, found the solidification front velocity to be of the order $O\left(10^{-4}\right)\,\text{cm/s}$, which is in full agreement with the velocity magnitude calculated using the two definitions of the Froude number proposed. For $\kappa \approx 4$, the grouping $(\kappa \cdot Fr_M)$ defined in the Λ term above may be calculated for a binary alloy system (Brass), and for the salt–water system (NH_4Cl–H_2O) to be $(\kappa \cdot Fr_M)_{Brass} = 3.82 \times 10^{-3}$ and $(\kappa \cdot Fr_M)_{Salt-Water} = 7.05 \times 10^{-8}$. So depending on the type of medium being solidified the parameter grouping $(\kappa \cdot Fr_M)$ could assume values in the region, $(\kappa \cdot Fr_M) \in \left[10^{-3}, 10^{-8}\right]$. In the current study we analyse solidifying systems for small Prandtl numbers (or small to moderate γ values) for the parameter grouping $(\kappa \cdot Fr_M)$ of the order $(\kappa \cdot Fr_M) = O\left(10^{-3}\right)$. The Prandtl number is defined as the ratio of the kinematic viscosity ν_* to the thermal diffusivity and is defined as $Pr = \nu_*/\lambda_*$. The dimensionless depth of the layer δ is the ratio of the height of the mushy layer H_* to the thermal diffusive length $l_{\lambda *}$ and is defined as $\delta = H_*/l_{\lambda *}$.

Following Anderson and Worster (1996) and Govender and Vadasz (2002), we may scale the dependent variables as in terms of the mushy layer depth δ as follows,

$$\boldsymbol{X} = \delta \tilde{\boldsymbol{X}}, \quad t = \delta^2 \tilde{t}, \quad R^2 = \delta Ra_m, \quad p = R\tilde{p}, \quad \boldsymbol{V} = \frac{R}{\delta}\tilde{\boldsymbol{V}}. \tag{10}$$

Applying the scalings in Equation (10) to Equations (5–6) and Equations (8–9) we obtain the following scaled system of governing equations,

$$\tilde{\nabla} \cdot \tilde{\boldsymbol{V}} = 0 \tag{11}$$

$$\left(\frac{\partial}{\partial \tilde{t}} - \delta \frac{\partial}{\partial \tilde{z}}\right)(T - St\varphi) + R\tilde{\boldsymbol{V}} \cdot \tilde{\nabla} T = \tilde{\nabla}^2 T \tag{12}$$

$$\left(\frac{\partial}{\partial \tilde{t}} - \delta \frac{\partial}{\partial \tilde{z}}\right)((1-\varphi)T - \varsigma\varphi) + R\tilde{\boldsymbol{V}} \cdot \tilde{\nabla} T = 0 \tag{13}$$

$$\frac{1}{(1-\varphi)\chi}\left(\frac{\partial}{\partial \tilde{t}} - \delta \frac{\partial}{\partial \tilde{z}}\right)\tilde{\boldsymbol{V}} + \Pi(\varphi)\tilde{\boldsymbol{V}} = -\tilde{\nabla}\tilde{p} + R\left[1 + \Lambda \text{Sin}(\Omega \tilde{t})\right] T \hat{e}_g \tag{14}$$

where $\chi = \delta^2 \chi_o = Da/Pr$. When the composition of the melt is close to that of the eutectic composition $(C_o - C_E \ll 1)$, a large concentration ratio, ς

is obtained. For this so-called near eutectic limit the concentration ratio may be defined as $\varsigma = C_s/\delta$, where C_S is the solid concentration and $\delta \ll 1$. Worster (1992) showed that for large concentration ratios ς, the permeability of the mushy layer is uniform/homogenous, and for this reason we set $\Pi(\varphi) = 1$, in the current analysis. We follow Anderson and Worster (1996) and define a large Stefan number, St, according to $St = \tilde{S}/\delta$.

3. Linear Stability Analysis

To establish the basic flow we need to analyse the equation set corresponding to the motionless state where the flow velocity is zero, and the temperature and solid fraction is horizontally uniform. Using an expansion in δ where the basic state has expansions:

$$[T_B, \boldsymbol{V}_B, \varphi_B, p_B] = [T_{BO}, \boldsymbol{V}_{BO}, \varphi_{BO}, p_{BO}] + \delta [T_{B1}, \boldsymbol{V}_{B1}, \varphi_{B1}, p_{B1}] + \delta^2 [T_{B2}, \boldsymbol{V}_{B2}, \varphi_{B2}, p_{B2}], \quad (15)$$

and a motionless state associated with basic flow implies that, $\boldsymbol{V}_B = 0$, $\partial T/\partial \tilde{t} = 0$, $\partial T/\partial \tilde{x} = 0$, $\partial T/\partial \tilde{y} = 0$, $\partial \varphi/\partial \tilde{t} = 0$, $\partial \varphi/\partial \tilde{x} = 0$ and $\partial \varphi/\partial \tilde{y} = 0$. Substituting Equation (15) in Equations (11–14) yields the motionless basic state solution for the temperature and solid fraction to each order of δ subject to the boundary conditions: $\tilde{z} = 0, T_B = -1$ and $\tilde{z} = 1, T_B = 0, \varphi_B = 0$,

$$T_B = T_{B0} + \delta T_{B1} = (\tilde{z} - 1) + \delta \left(-\frac{(1 + \tilde{S}/C_s)}{2} \tilde{z}^2 + \frac{2 + (1 + \tilde{S}/C_s)}{2} \tilde{z} - 1 \right), \quad (16)$$

$$\varphi_B = \delta \varphi_{B1} + \delta^2 \varphi_{B2} = (\tilde{z} - 1) + \delta \left(\frac{1 - \tilde{z}}{C_s} \right) + \delta^2 \left(\frac{1}{C_s} \left(\frac{1}{2} \left(\frac{2}{C_s} + \left(1 + \tilde{S}/C_s \right) \right) \tilde{z}^2 - \left(1 + \frac{(1 + \tilde{S}/C_s)}{2} + \frac{2}{C_s} \right) \tilde{z} + 1 + \frac{1}{C_s} \right) \right). \quad (17)$$

It can be observed from Equation (17) that to $O(\delta^0)$, $\varphi_{B0} = 0$. This result clearly shows that for $\delta \ll 1$, a small amount of solid is formed for the near eutectic approximation. To analyse the stability of the basic state solution (16, 17) we apply small perturbations about of the form,

$$[T, \boldsymbol{V}, \varphi, p] = [T_B, 0, \varphi_B, p_B] + \varepsilon [T_1, \boldsymbol{V}_1, \varphi_1, p_1] + \varepsilon^2 [T_2, \boldsymbol{V}_2, \varphi_2, p_2], \quad (18)$$

where $\varepsilon \lll 1$, as required by the linear theory. For the particular case when $\delta = O(\varepsilon)$, we note that the basic state solution, Equation (15), now interacts with the perturbed terms in Equation (18). As a result Equation

(18) may be re-written as follows for the case $\delta = O(\varepsilon)$,

$$[T, \boldsymbol{V}, \varphi, p] = [T_{B0}, 0, 0, p_{B0}] + \varepsilon [(T_1 + T_{B1}), (\boldsymbol{V}_1 + \boldsymbol{V}_{B1}), (\varphi_1 + \varphi_{B1}), (p_1 + p_{B1})] + \varepsilon^2 [(T_2 + T_{B2}), (\boldsymbol{V}_2 + \boldsymbol{V}_{B2}), (\varphi_2 + \varphi_{B2}), (p_2 + p_{B2})]. \quad (19)$$

Solving the Equation set (11–14) for the perturbation definition proposed in Equation (19) to $O(\varepsilon)$ yields

$$\frac{\partial T_1}{\partial t} + R w_1 - 1 = \frac{1}{\eta_o} \nabla^2 T_1, \quad (20)$$

$$\left[\frac{1}{\chi} \frac{\partial}{\partial t} + 1 \right] V_1 = -\nabla p_1 - R [1 + \Lambda \sin(\Omega t)] T_1 \hat{e}_z = 0, \quad (21)$$

where $\eta_o = 1 + \tilde{S}/C_s$.

Following Govender (2004a), we apply the curl operator twice on Eq.(21) in order to eliminate the pressure term, and only consider the z-component of the result as follows,

$$\left[\frac{1}{\chi} \frac{\partial}{\partial t} + 1 \right] \nabla^2 w_1 + R [1 + \Lambda \sin(\Omega t)] \nabla_H^2 T_1 = 0, \quad (22)$$

where $\nabla_H^2 \equiv \partial^2/\partial x^2 + \partial^2/\partial y^2$ and w_1 is the perturbation to the vertical component of the filtration velocity. Equations (20) and (22) may be decoupled by eliminating w_1 providing a single equation for the temperature perturbation T_1 in the form,

$$\left[\frac{1}{\chi} \frac{\partial}{\partial t} + 1 \right] \nabla^2 \left[\frac{\partial}{\partial t} - \frac{1}{\eta_o} \nabla^2 \right] T_1 - R^2 [1 + \Lambda \sin(\Omega t)] \nabla_H^2 T_1 = 0 \quad (23)$$

Assuming an expansion into the normal modes in the x- and y-directions, and a time dependent amplitude $\theta(t)$ similar to that of Govender (2004a), we obtain

$$T_1 = \theta(t) e^{i(s_x x + s_y y)} \sin(\pi z) + c.c. \quad (24)$$

where again $c.c.$ represents the complex conjugate terms and $s^2 = s_x^2 + s_y^2$. Substituting Equations (24) into (23) yields,

$$\frac{d^2\theta}{dt^2} + 2p \frac{d\theta}{dt} - F(\alpha)\gamma \left[(\hat{R} - \hat{R}_o) + \hat{R} \Lambda \mathrm{Sin}(\Omega t) \right] \theta = 0 \quad (25)$$

where $\alpha = s^2/\pi^2$, $\gamma = \chi/\pi^2$, $\hat{R} = \tilde{R}^2$, $\tilde{R} = R/\pi^2$, $\hat{R}_o = \tilde{R}_o^2$, $\tilde{R}_o = R_o/\pi^2$, R_o is the un-modulated Rayleigh number defined as $\tilde{R}_o = \pi^2(\alpha + 1)^2 \eta_o \alpha$, $2p = \pi^2 [(\alpha + 1)\eta_o + \gamma]$ and $F(\alpha) = \pi^6 \alpha/(\alpha + 1)$. Using the transformation

$t = (\pi/2 - 2\tau)/\Omega$, Equation (25) may be cast, as indicated by McLachlan (1964), into the canonical form of the Mathieu equation:

$$\frac{d^2X}{d\tau^2} + [a + 2q\cos(2\tau)]\,X = 0 \tag{26}$$

The solution to Equation (26) follows the form $G(\tau) = e^{-\sigma\tau}\chi(\tau)$ where $G(\tau)$ is a periodic function with a period of π or 2π and σ is a characteristic exponent which is a complex number, and is a function of a and q, respectively (See Govender (2004a)). In this paper the definitions for a, q and σ are obtained upon transforming Equation (25) into the canonical form of Mathieu's equation, and are defined as,

$$\frac{2}{\sqrt{-a}} = \frac{\Omega}{\left[F(\alpha)\gamma(\hat{R} - \eta)\right]^{1/2}}, \tag{27}$$

$$\frac{1}{2}q = F(\alpha)\gamma\hat{R}\kappa Fr, \tag{28}$$

$$\sigma = -\frac{2p}{\Omega} \tag{29}$$

$$\eta = -\frac{\hat{R}_o\eta_o}{4\gamma(\alpha+1)}\left[\frac{\alpha+1}{\eta_o} - \gamma\right]^2 \tag{30}$$

When $\sigma = 0$, the solution to Equation (26) is defined in terms of Mathieu functions, c_e and d_f (where $e = 1, 2, 3, \ldots, E$ and $f = 1, 2, 3, \ldots, F$), such that for each Mathieu function, c_e and d_f, there exists a relation between a and q. This relationship is shown by Govender (2004b) for the Mathieu function d_o, c_1 and d_1. One would observe alternating stable and unstable zones if various Mathieu functions, c_e and d_f, are plotted on the same set of axes. In the stable regions of Mathieu's equation, σ is complex with a negative real part. Since σ is a function of a and q, which are dependent on γ, $\hat{R}$, α, Λ and Ω, the stability of the mushy layer is also seen to depend on these variables as well. In addition there are solutions to Equation (26) for $a > 0$ and $a < 0$; also, q may be replaced by $-q$ with no effect on the solution. In this study for a solidifying binary alloy the numerical values for "a" are less than zero and are defined by Equation (27). We also propose the following definition for the modified characteristic exponent, $\xi = \sigma/\sqrt{-a}$. A chart of $1/2q$ versus $2/\sqrt{-a}$ for various values of ξ is shown in Figure 2 for small values of q, see McLachlan (1964). We may now present a relation for the characteristic Rayleigh number in terms of the newly defined parameter ξ, by substituting $\xi = \sigma/\sqrt{-a}$ in Equation (27), and rearranging to yield,

$$\hat{R} = \frac{\hat{R}_o - \eta}{\xi^2} + \eta. \tag{31}$$

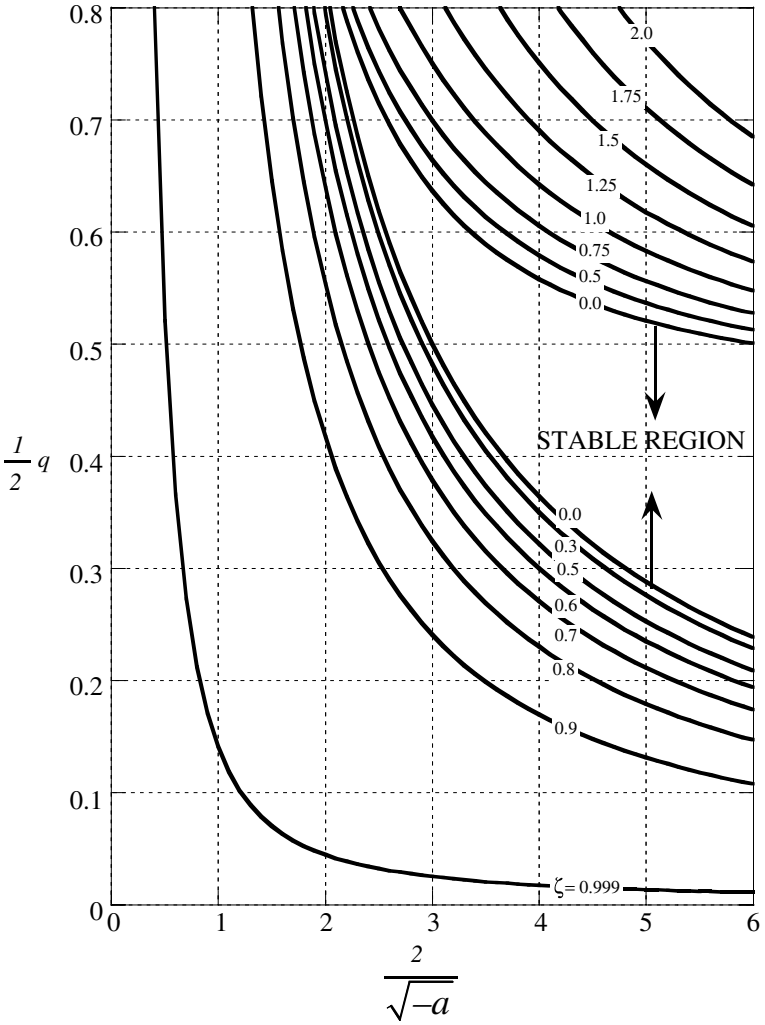

Figure 2. Stability chart for Mathieu equation presented as $1/2q$ versus $2/\sqrt{-a}$, for various values of the modified exponent ξ.

Figure 2 together with Equations (27–30) and (31) may be used to evaluate the critical Rayleigh number and wavenumbers in terms of the frequency, Ω, the parameter κFr and γ. We proceed, in a similar fashion to Govender (2004a), by first evaluating the characteristic Raleigh number versus the frequency for selected values of the wavenumber according to the following method: (a) select a value of ξ, (b) evaluate $\hat{R}$ using Equation (36), (c) compute the value for $1/2q$ using Equation (35), (d) read $2/\sqrt{-a}$ from Figure 2, and (e) evaluate the frequency from Equation (32). The results of the process outlined in steps 1 to 5 above are depicted in

Figure 3 for parameter values $\gamma = O(1.5)$ and $(\kappa Fr) = O(10^{-3})$. In Figure 3, for any selected wavenumber, it is noted that the stable zone is below the curve whilst the unstable zone is above the curve. An example of the location of the unstable and stable regions is shown in Figure 3 for $\alpha = 1.5$. Using the results in Figure 3 we may evaluate the critical wave number and Rayleigh number for numerous values of wave number α across a bandwidth of frequencies.

The effect of the important ratio $\tilde{S}/C_s$ (embodied in the term η_o) on the critical Rayleigh number and frequency is shown in Figure 4 for selected η_o values, viz. $\eta_o = 1, 1.5$, and 2 at $\gamma = O(1.5)$ and $(\kappa Fr) = O(10^{-3})$. It can be observed from Figure 4 that as η_o increases from 1 to 2 the convection becomes destabilised across the indicated bandwidth of frequencies. The

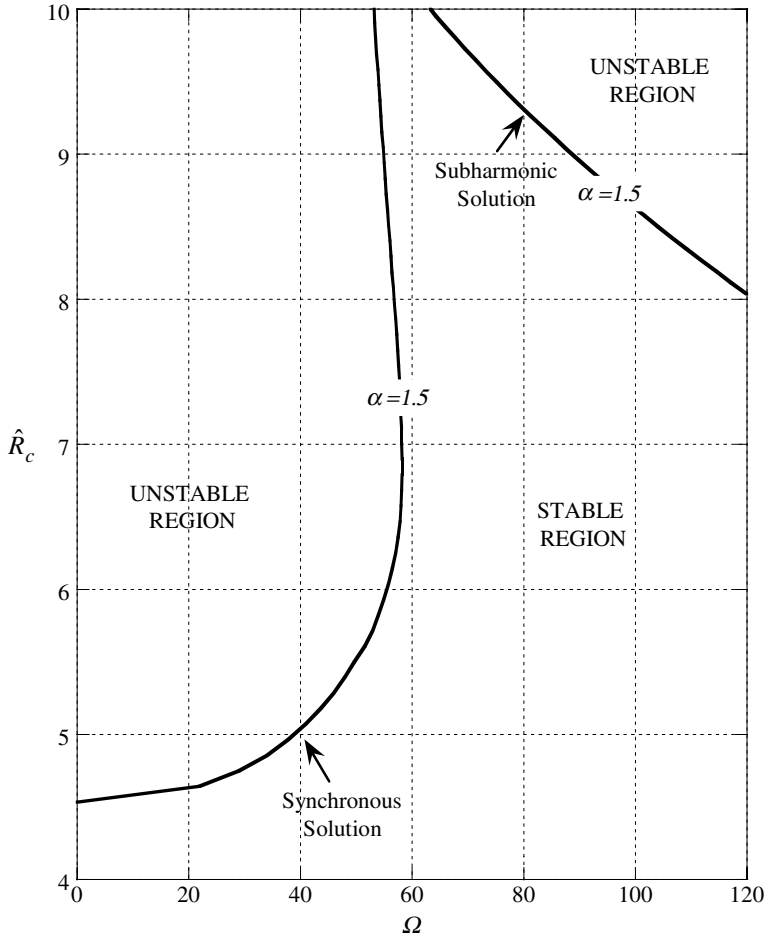

Figure 3. Characteristic Rayleigh number versus the scaled vibration frequency for selected values of wavenumber.

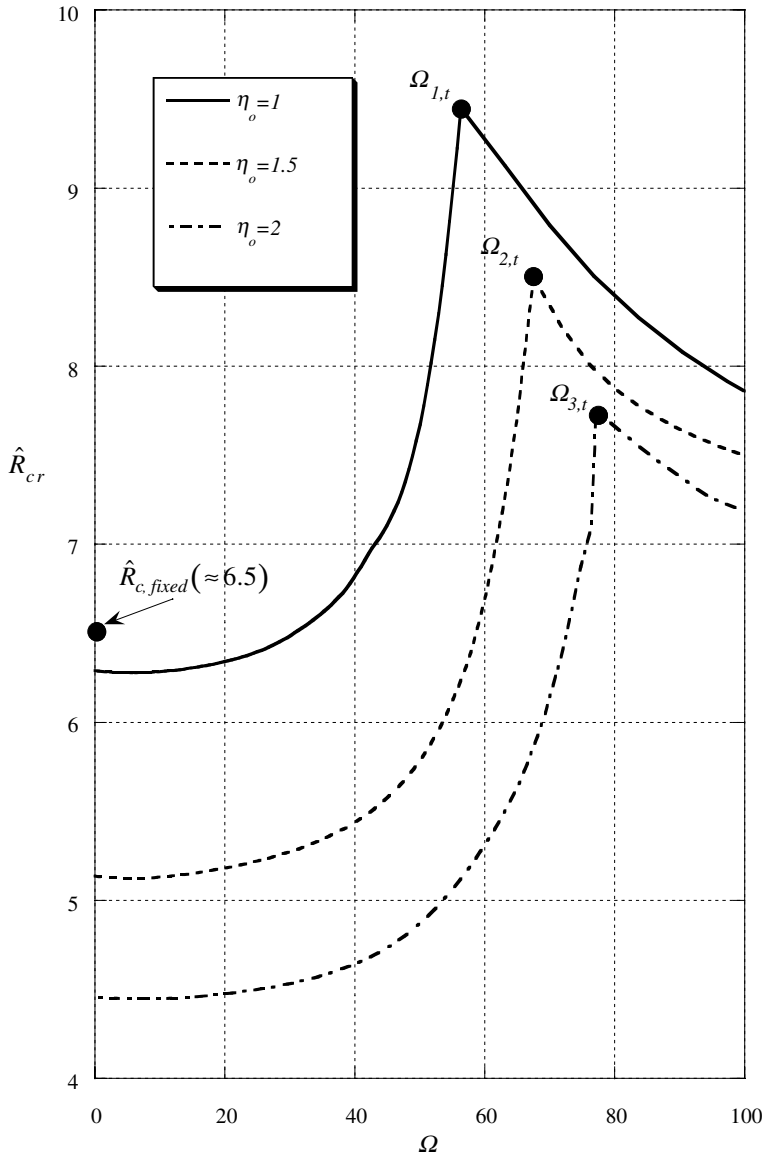

Figure 4. Critical Rayleigh number versus the scaled vibration frequency for various values of the parameter η_o at $\gamma = O(1.5)$ and $(\kappa Fr) = O(10^{-3})$.

setting $\eta_o = 1$ corresponds to the case when the Stefan number equals zero (i.e. there is no solidification), whilst $\eta_o = 2$ corresponds to the case $\tilde{S} = O(C_s)$ (or $St = O(\varsigma)$). Calculations were performed for numerous values of η_o and it was found that beyond $\eta_o = 10$ no solutions are found to exist. The results in general follow similar trends to that generated by Govender

(2004b), but the transition points $\Omega_{1,t}, \Omega_{2,t}, \Omega_{3,t}$ (from synchronous to subharmonic solutions for each η_o value) occur at significantly lower frequencies. In addition the stabilising effect of vibration occurs over a bandwidth of lower frequency values in comparison to that of the passive porous layer investigated by Govender (2004a). This is a welcomed result as high frequency vibration will initiate macro-segregation in the solidifying alloy and defeat the objective of using vibration to stabilise the solutal convection. Bearing in mind that for solidification to occur we require that $\eta_o > 1$, it is quite clear from the curves presented in Figure 4 that the process of solidification (i.e. increasing Stefan number) destabilises the convection.

The results shown in Figure 4 may be used by a plant metallurgical engineer to control suppress the onset of solutal convection using vibration. Worster (1992) showed that the onset of solutal convection results in the creation of freckles/channels in the final solidified ingot, which has a negative impact on the mechanical strength of any object produced from the ingot. For this reason it is critical that solutal convection is suppressed or negated altogether during the solidification process. If during the casting process the characteristic Rayleigh number is $R_{c,fixed} \approx 6.5$ for a particular composition (as indicated on Figure 4), for $\gamma = O(1.5)$ and $(\kappa Fr) = O(10^{-3})$, then one may observe that for, say $\eta_o = 2$, the critical Rayleigh number for the onset of solutal convection has been exceeded for $\Omega = 0$. In order to suppress the solutal mode of convection for the given parameter settings, the metallurgical engineer would have to ensure that the vibration frequency of the crucible containing the solidifying system is greater than $\Omega \approx 75$. If the system being cast exhibits a Darcy–Prandtl number (γ) other than $\gamma = O(1.5)$, then the curves provided in Figure 4 will have to be re-generated and re-analysed as mentioned above for the selected γ value. Incidentally the effect of increasing the γ value for any selected value of η_o is to destabilise the solutal convection corresponding to the subharmonic region, and to stabilise the convection in the synchronous region. It must be borne in mind that for binary alloy solidification, one is concerned with using low frequency vibration to prevent undesired effects such as macro-segregation. For this reason it is anticipated that the region of synchronous solutions will be sufficient for use in casting applications.

4. Conclusion

The current study investigates the effect of gravity modulation on the stability of solutal convection in the mushy layer of a solidifying binary alloy. A linear stability analysis is performed with the aid of the Mathieu stability charts and the results of the study shows that low amplitude gravity modulation stabilizes the solutal convection. It was also discovered that stabilizing effect of vibration on solutal convection occurs at relatively low

frequencies, and it was also discovered that increasing the ratio of Stefan number to solid composition tends to destabilize the solutal convection. It was also demonstrated that the effect of increasing the Darcy–Prandtl number is to stabilise the convection in the subharmonic region and destabilize the convection in the synchronous region.

Acknowledgements

The author would like to thank the National Research Foundation (NRF) for funding this research through the THUTUKA Program (REDIBA – GUN: 2053945)

References

Amberg, G. and Homsy, G. M.: (1993), Nonlinear analysis of buoyant convection in binary solidification with application to channel formation, *J. Fluid Mech*. **252**, 79–98.

Anderson, D. M. and Worster, M. G.: (1995), A new oscillatory instability in mushy layers during the solidification of binary alloys, *J. Fluid Mech*. **307**, 245–267.

Anderson, D. M. and Worster, M. G.: (1996), Weakly nonlinear analysis of convection in mushy layers during the solidification of binary alloys, *J. Fluid Mech*. **302**, 307–331.

Chen, C. F. and Chen, F.: (1991), Experimental study of the directional solidification of aqueous ammonium chloride solution, *J. Fluid Mech*. **227**, 567–586.

Chen, F., Lu, J. W. and Yang, T. L.: (1994), Convective instabilities in ammonium chloride solution directionally solidified from below, *J. Fluid Mech*. **276**, 163–187.

Copey, S. M., Giamei, A. F., Johnson, S. M. and Hornbecker, M. F.: (1970), The origin of freckles in unidirectional solidified castings, *Metall. Trans*. **1**, 2193–2204.

Fowler, A. C.: (1985), The formation of freckles in binary alloys, *IMA J. Appl. Maths* **35**, 159–174.

Govender, S.: (2004a), Stability of convection in a gravity modulated porous layer heated from below, *Transport Porous Media* (in press).

Govender, S.: (2004b), Stability of convection in a gravity modulated porous layer heated from below: transition from synchronous to subharmonic solutions, *Transport Porous Media (Under Review)*.

Govender, S. and Vadasz, P.: (2002), Moderate time linear stability of moderate Stefan number convection in rotating mushy layers, *J. Porous Media* **5**(2), 113–121.

McLachlan, N. W.: 1964, *Theory and Application of Mathieu Functions*, Dover, New York.

Nield, D. A.: (1999), Modelling effects of a magnetic field or rotation on flow in a porous medium, *Int. J. Heat and Mass Tran*. **42**, 3715–3718.

Tait, S. and Jaupart, C.: (1992), Compositional convection in a reactive crystalline mush and melt differentiation, *J. Geophys. Res*. **97**(B5), 6735–6756.

Vadasz, P.: 1998, Coriolis effect on gravity-driven convection in a rotating porous layer heated from below, *J. Fluid Mech.* **376**, 351–375.

Worster, M. G.: (1992), Instabilities in the mushy regions during solidification of alloys, *J. Fluid Mech*. **237**, 649–669.